FULL PAPER

Hematite Films Decorated with Nanostructured Ferric Oxyhydroxide as Photoanodes for Efficient and Stable Photoelectrochemical Water Splitting

*Qing Yu, Xianguang Meng, Tao Wang, Peng Li, and Jinhua Ye**

Hematite photoanodes are decorated with nanostructured FeOOH by photoelectrodeposition. An obvious cathodic shift in the photocurrent onset potential is observed, while four-times enhancement of photocurrent density enhancement is acheived with FeOOH present. This can be ascribed to the high reaction area for the structure and high electrocatalytic activity of nanostructured FeOOH, which increases the amount of photogenerated holes involved in the water oxidation reaction and accelerates the kinetics of water oxidation. Furthermore, the obtained Fe_2O_3/FeOOH photoanode achieves considerable O_2 evolution rate (10.1 μmol h^{-1} cm^{-2}) under AM 1.5 G illumination and is maintained for as long as 70 h. The Fe_2O_3/FeOOH films show visible light response, high photocurrent density, and long-term stability, and they are well qualified photoanode materials and a promising candidate for photoelectrochemical water splitting.

1. Introduction

Due to the increasing global demand for energy, as well as the awareness of climate change, searching for clean energy source especially taking advantage of the enormous amount of solar energy becomes urgent. Using photoelectrochemical (PEC) photocells to produce hydrogen and oxygen from pure water provides a good candidate for solar energy conversion.[1] In the past few years, a number of exceptional n-type semiconductors have been widely researched as photoanodes for oxygen evolution, such as TiO_2,[2] Fe_2O_3,[3] $BiVO_4$,[4] and (oxy)nitrides[5] due to their enough positive valence band positions.[6,7b] Among all these materials, hematite (α-Fe_2O_3) is one of the most attractive candidates for PEC water oxidation reaction because of its suitable band gap (2.0–2.1 eV) to absorb visible light, excellent stability in aqueous and under water oxidation conditions, nontoxic, and earth-abundant.[7–9] However, the low conductivity, limited carrier life time, short hole diffusion length (2–4 nm) and high electron–hole recombination rate of hematite have prevented the performance for solar energy conversion.[10–12] Consequently, it is preferable to prepare films of a few nanometers so that the photogenerated holes can be transferred to the electrode/electrolyte interface before recombination with electrons. Providing high reaction area for efficient light harvesting towards these thin absorber films (hematite based films) is an effective approach to overcome the above-mentioned disadvantages.

Generally, loading oxygen evolution catalysts on the surface is one of the most popular methods to lower oxygen evolution reaction (OER) barrier of hematite photoanode materials, which has obtained considerable progresses due to rich selections in such kind of materials for matching.[13] Various materials have been studied and deposited to the surface of hematite, including IrO_2,[14] cobalt phosphate (Co-pi),[15] nickel(II) hydroxide,[16] and $NiFeO_x$ layers.[17] Although these OER catalysts have expressed reduce of onset potential to bare hematite for water oxidation, some of them are restricted for their unstable property or having competing light absorbance in the visible light region. Furthermore, the whole photoelectrodes should not contain any rare elements, so OER catalysts such as RuO_x and IrO_x were not good choices considering the possibility for further practical use. Ferric oxyhydroxide (FeOOH) have been studied by several groups in recent years since Fe element is very abundant in the earth just after Si, Al, and O. In addition, it is stable at water oxidation conditions in neuter and alkaline conditions. As a result, it has been applied to some potential photoanodes, including Si,[18] $BiVO_4$[4] and has shown improvement performances in both onset potentials and photocurrent densities. In this work, flat hematite films were prepared by pulsed laser deposition (PLD) on indium tin oxide (ITO) substrate and were subsequently coated with nanostructured FeOOH by photoelectrodeposition. After decorating

Q. Yu, X. Meng, Prof. J. Ye
Graduate School of Chemical Science and Engineering
Hokkaido University
Sapporo 060-0814, Japan
E-mail: jinhua.ye@nims.go.jp
Q. Yu, X. Meng, Dr. T. Wang, Dr. P. Li, Prof. J. Ye
International Center for Materials Nanoarchitectonics (WPI-MANA) and Environmental Remediation Materials Unit
National Institute for Materials Science (NIMS)
1-1 Namiki, Tsukuba, Ibaraki 305-0044, Japan
Prof. J. Ye
TU-NIMS Joint Research Center
School of Materials Science and Engineering
Tianjin University
92 Weijin Road, Tianjin, P.R. China
Prof. J. Ye
Collaborative Innovation Center of Chemical Science and Engineering (Tianjin)
Tianjin 300072, P.R. China

DOI: 10.1002/adfm.201500383

FeOOH cocatalyst, the onset potential had a cathodic shift about 140 mV. It is observed that the FeOOH does not compete with hematite for light absorption while demonstrates remarkable enhancement for photocurrent density to more than four times of the bare Fe_2O_3 photoanodes. The obtained Fe_2O_3/FeOOH photoanodes achieved quite high oxygen evolution rate from PEC water splitting, which was 10.1 μmol h^{-1} cm^{-2} at 0.43 V versus normal hydrogen electrode (NHE) (1.23 V vs reversible hydrogen electrode (RHE)) under air mass 1.5 G (AM 1.5 G) illumination for as long as 70 h. Overall, the nanostructured FeOOH decorated Fe_2O_3 photoanode (simplified as Fe_2O_3/FeOOH) was first obtained with high water oxidation rate and durability and showed great potentials as an all-Fe-based photoanode for PEC water oxidation.

2. Results and Discussion

The details for preparing Fe_2O_3 films by PLD have been illustrated in our previous articles.[19] The freshly prepared Fe_2O_3 photoanode showed relatively lower photocurrent compared with other reports because the films fabricated by PLD are generally smooth with low reaction area. In order to improve the efficiency of the photo generated holes to oxygen and lower the overpotential of Fe_2O_3 photoanode, FeOOH were deposited by photoelectrodepositon from $FeSO_4$ solution as previous reports.[4] The cyclic-voltammetry (CV) curves of $FeSO_4$ solution baths on Fe_2O_3 are shown in Figure S1a, Supporting Information. Based on the CV curves, the voltage for FeOOH deposition from $FeSO_4$ was fixed on 0.2 V versus Ag/AgCl under AM 1.5 G illumination. Representative current–time trace for FeOOH deposition is shown in Figure S1b, Supporting Information. After the deposition of FeOOH on the surface of Fe_2O_3, the whole piece was put into the oven and annealed at 300 °C in air for 2 h. FeOOH with different amount were fabricated to optimize the maximum photocurrent (Figure S2a, Supporting Information). It is demonstrated that Fe_2O_3 photoanode with 6.5 mC cm^{-2} amount of nanostructured FeOOH showed the best improvement in photocurrent density and onset potential. As a result, in the following experiments, the FeOOH cocatalyst was maintained with amount of 6.5 mC cm^{-2}, which were obtained by photoelectrodeposition under 0.2 V versus Ag/AgCl applied bias for 1 h. The surface morphology of bare Fe_2O_3 and Fe_2O_3 loaded with different amount of FeOOH cocatalyst are shown in **Figure 1**. The amount of FeOOH for samples in Figure 1b–d were 3.4, 6.5, and 12.7 mC cm^{-2}, respectively. So the sample shown in Figure 1c had the maximum photocurrent density among the three samples. It is observed that the surface morphology of Fe_2O_3 and FeOOH were quite different. The surface of Fe_2O_3 showed a relatively smooth morphology (Figure 1a), and the average roughness was only ≈4.5 nm (Figure S3, Supporting Information). While in the initial stage of deposition, the FeOOH was in form of nanosheet (Figure 1b,c) with thickness only ≈15 nm (inset in Figure 1c). The thicknesses of FeOOH layer were ≈70 and ≈100 nm, respectively, as shown in Figure S4, Supporting Information. As a result, with deposition time increased, not only the thickness but also the density of FeOOH layer was increased. Since the FeOOH nanosheets were grown cross the surface of Fe_2O_3, the rugged surface formed would increase the reaction area of the photoanodes. Besides, after uniformly covering by FeOOH, the reaction area increased with the deposition time extending.

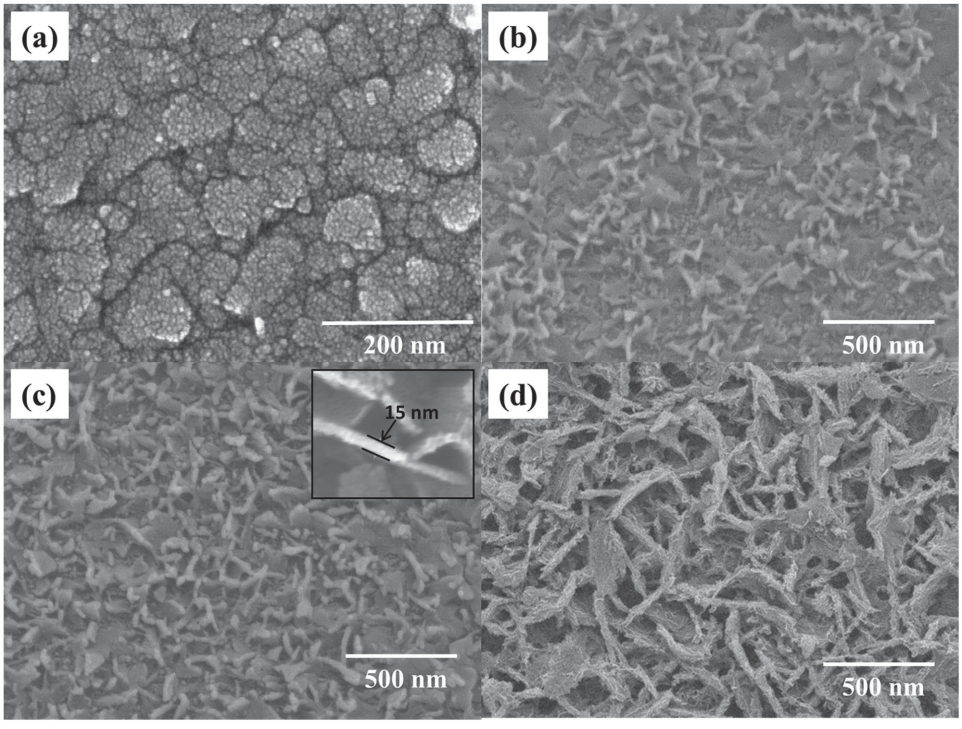

Figure 1. SEM (scanning electron microscope) images of a) bare Fe_2O_3, b–d) Fe_2O_3 with different amount of FeOOH. The amount of FeOOH for (b–d) are 3.4, 6.5, 12.7 mC cm^{-2}, respectively.

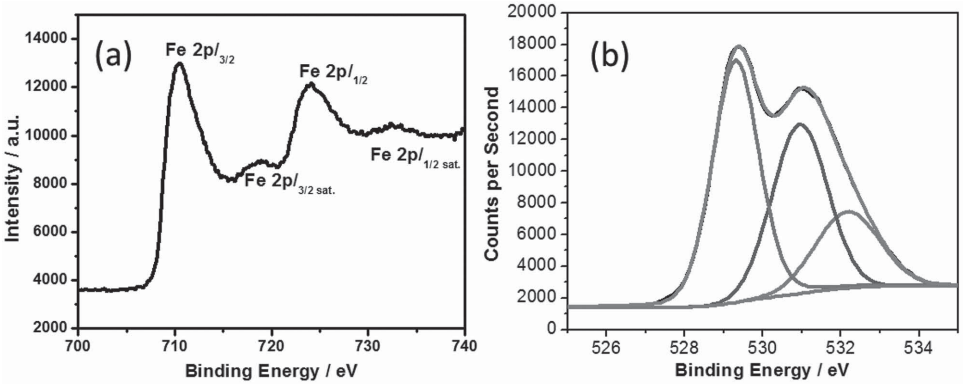

Figure 2. XPS spectrums of a) Fe (2p) and b) O (1s) for FeOOH.

However, when FeOOH reached a certain amount, the particles of FeOOH grew bigger. The FeOOH were no longer in form of nanosheets, but like ribbons which covered almost the whole surface of Fe_2O_3.

As no peaks of FeOOH can be found from the x-ray diffraction (XRD), the FeOOH were likely to be amorphous and were characterized by x-ray photoelectron spectroscopy (XPS) (**Figure 2**) and Raman spectroscopy (Figure S5, Supporting Information). The composition of FeOOH cocatalyst was characterized by XPS (Figure 2). From the XPS spectra of Fe (2p), Fe^{3+} is obviously found. And it indicates that almost all the Fe^{2+} in $FeSO_4$ was oxidized to Fe^{3+} during the deposition process. In the region of O (1s) in XPS spectra, there are three strong peaks. The lower peak (529.3 eV) is attributed to O^{2-} species while the higher peak (531.0 eV) is attributed to OH^-. The peak at 532.0 eV is attributed to adsorbed water.[18] In order to get more insight into the as prepared FeOOH cocatalyst, Raman spectroscopy was used. The sample for Raman characterization was deposited for 12 h to get a relatively strong signal. The combination of clear peaks at 475 and 1000 cm^{-1} are easily distinguished from other iron (oxy)hydroxide spectrums indicating goethite (α-FeOOH) was obtained in our experiments (Figure S5, Supporting Information).[18a] The peaks were broad. This is because the goethite prepared by photoelectrodeposition was amorphous in which only a short range order exists.[18b,c] Besides, no sulfur peak is found in the energy dispersive spectrometer (EDS) spectra as shown in Figure S6, Supporting Information. From all the results discussed above, the $FeSO_4$ was totally transformed into FeOOH on the surface of Fe_2O_3 after deposition and postannealing.

The absorption spectrums of Fe_2O_3 photoelectrodes with or without nanostructured FeOOH are shown in Figure S7, Supporting Information. The absorption region of FeOOH is below 350 nm, indicating the FeOOH are not able to compete with Fe_2O_3 for the light absorption in the visible light region. Current–potential curves of bare FeOOH were further used to make sure whether it made any contribution to the photocurrent density (Figure S8, Supporting Information). The current–potential curve in the dark and light was nearly the same, meaning the nanostructured FeOOH have very weak light response under light irradiation which can almost be neglected. As a result, the photogenerated holes for water oxidation in Fe_2O_3/FeOOH photoanodes are mainly come from the Fe_2O_3 layer prepared by PLD, while the nanostructured FeOOH are only functioned as cocatalyst to increase the amount of holes involved in the water oxidation reaction.

Details about comparison of the PEC performance between Fe_2O_3 with or without FeOOH present are shown in **Figure 3**. Linear-sweep-voltammetry (LSV) sweeps for Fe_2O_3/FeOOH photoanode were performed in 1 M NaOH solution both in dark and light under AM 1.5 G illumination (Figure 3a), with similar tests for bare Fe_2O_3 as reference. The current density had increased a lot after coating nanostructured FeOOH cocatalyst. While the onset potential of Fe_2O_3 shifted negatively from ≈0.13 to ≈0 V after FeOOH decoration. To quantitatively value the amount of cathodic shift on onset potential from the FeOOH decorated Fe_2O_3 photoanode, we further analyzed the LSV curve (Figure 3a) according to the report by Formal[20] and Wang.[17] First, the differential curve between potential and current density was made. And then the onset potential is defined as the value at which $dJ/dV > 0.2$ mA cm^{-2} V^{-1} (Figure 3b). The onset potential for bare Fe_2O_3 was 0.08 V while the onset potential for FeOOH decorated Fe_2O_3 was –0.06 V. As we can see, the 140 mV potential shifts are almost consistent with the current–potential curves as shown in Figure 3a. To examine the photoresponse of the nanostructured FeOOH decorated Fe_2O_3 over time, *I–t* curve of Fe_2O_3/FeOOH at 0.43 V versus NHE (1.23 V vs RHE) was measured (Figure 3c). Once the light was turned on, a spike in the photoresponse can be observed for all the samples because of the rapid effect upon power excitation, but the photocurrent quickly turned back to a steady state within 1 s.

The nanostructured FeOOH decorated Fe_2O_3 exhibited superior PEC performance, increased photocurrent density and decreased onset potential. The highly improved current density was partly owed to the nanostructured FeOOH. Besides, the contact between FeOOH cocatalyst and Fe_2O_3 were quite good, so that the recombination rate of electron-hole pairs was maintained at a low range at the Fe_2O_3/FeOOH interface. The decreased recombination rate also made the current density increased significantly.

Moreover, it is proposed that the existence of FeOOH decreased the reaction barriers for water oxidation and facilitated the holes transfer to the electrode/electrolyte interface, accounting for the greatly improved PEC performance. It is commonly known that the electrochemical impedance spectroscopy (EIS) analysis provides information about the interfacial

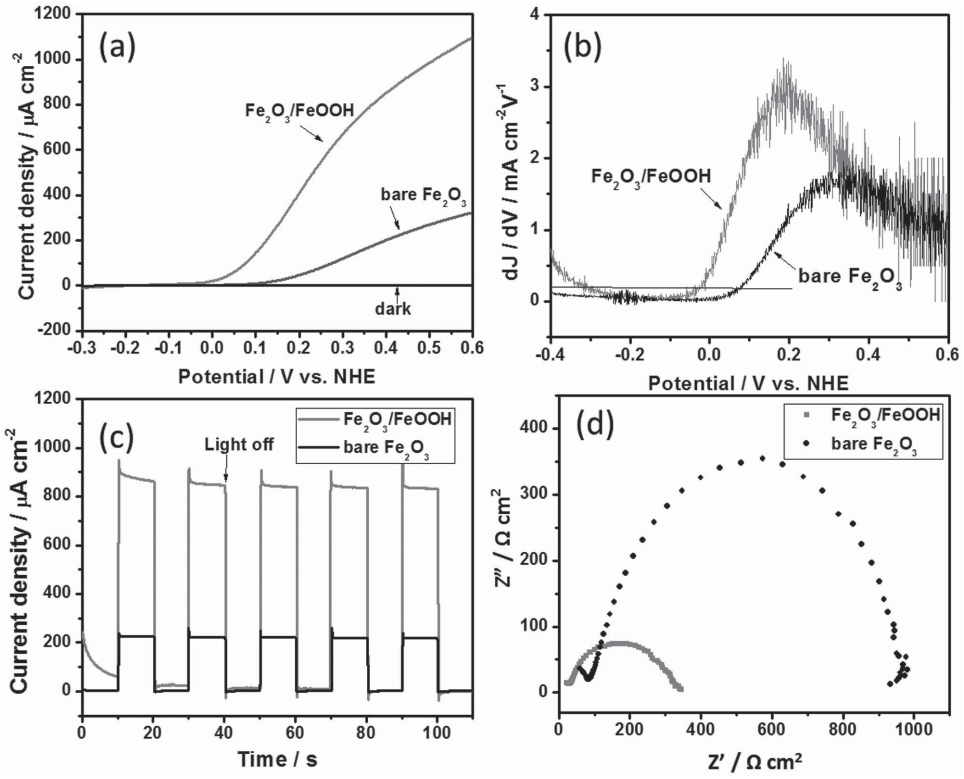

Figure 3. Comparison of the PEC performances of Fe_2O_3 with or without FeOOH in 1 M NaOH (pH = 13.6) solution. a) Current–potential curves under AM 1.5 G illumination. b) First-order derivative of the photocurrent density as a function of voltage. V_{on} is defined as the value at which $dJ/dV > 0.2$ mA cm^{-2} V^{-1}. c) Current–time curves at 0.43 V versus NHE under AM 1.5 G illumination. d) Nyquist plots measured under the same illumination at 0.43 V versus NHE.

properties of electrodes.[21] The diameter of the semicircle in EIS equals the electron transfer resistance, which subjects the electron transfer kinetics of the redox probe at the electrode interface.[21] Figure 3d shows the typical EIS curve for bare Fe_2O_3 photoanode and Fe_2O_3/FeOOH photoanode in 1 M NaOH under illumination, respectively. A smaller diameter is observed in the curve of Fe_2O_3/FeOOH photoanode under illumination relative to bare Fe_2O_3, which means the resistance between FeOOH/electrolyte interface was much smaller than the Fe_2O_3/electrolyte interface. This indicates a conducting effect of the FeOOH on the charge–transfer process which would decrease the charge transfer barrier at the electrode interface. As a result, the oxygen evolution reaction barrier was reduced by decreasing the charge transfer barrier as reported in previous reports.[22–24] Water oxidation was easier to realize due to the decreased reaction barrier, so a cathodically shift appeared in the onset potential.

The effect of FeOOH on enhancing PEC performance of Fe_2O_3 was further confirmed by comparing the potential providing the same current density (0.5 mA cm^{-2}) as well as the current density at the same applied voltage (0.43 V vs NHE) as shown in **Figure 4**. The potentials to generate current density

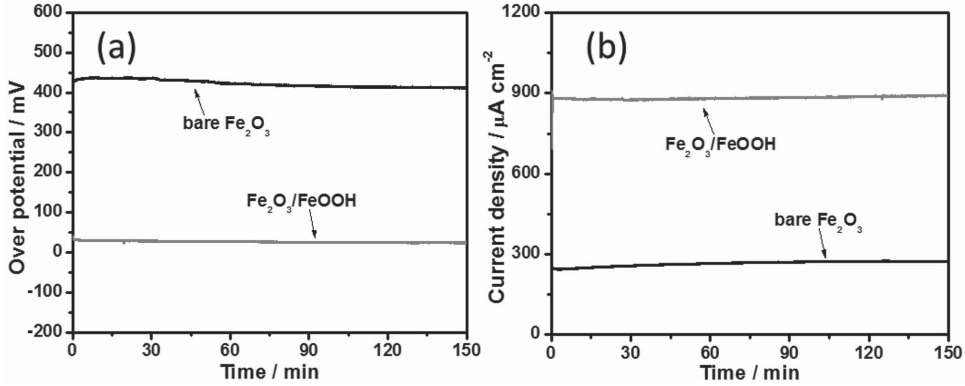

Figure 4. a) Potential (V vs Ag/AgCl) versus time for Fe_2O_3 and Fe_2O_3/FeOOH, respectively, at 0.5 mA cm^{-2}. b) Photocurrent obtained at 0.43 V versus NHE of Fe_2O_3 and Fe_2O_3/FeOOH, respectively. The solution is 1 M NaOH (pH = 13.6) while the light source is AM 1.5 G illumination.

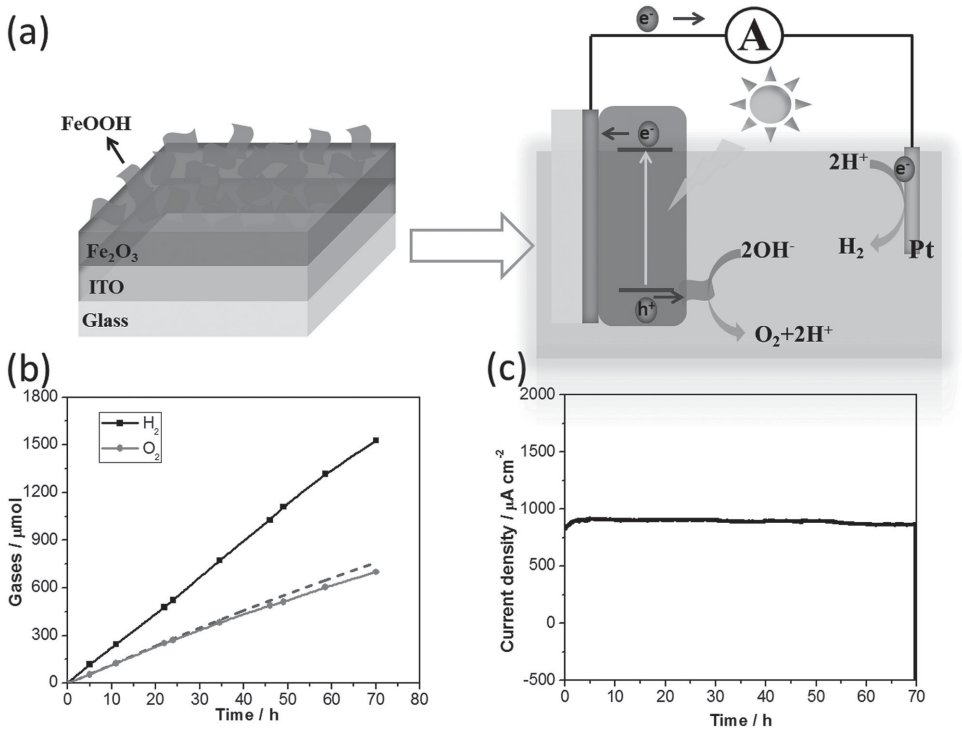

Figure 5. a) Schematic view of Fe_2O_3/FeOOH photoanodes and their energy diagram for PEC water splitting. b) Long-time gas evolution curves for FeOOH decorated Fe_2O_3 photoelectrode under AM 1.5 G illumination at 0.43 V versus NHE (1.23 V vs RHE), and c) corresponding *I–t* curve. Broken line in (b) is the amount of O_2 calculated from photocurrent in (c) assuming 100% faradaic efficiency.

about 0.5 mA cm^{-2} for Fe_2O_3 and Fe_2O_3/FeOOH photoanodes were 0.63 V versus NHE (0.43 V vs Ag/AgCl) and 0.23 V versus NHE (0.03 V vs Ag/AgCl), respectively (Figure 4a). Besides, the photocurrent density at 0.43 V versus NHE (1.23 V vs RHE) for bare Fe_2O_3 was only 217 μA cm^{-2}. However, when nanostructured FeOOH was decorated on the surface of Fe_2O_3 with appropriate amount (6.5 mC cm^{-2}), the photocurrent reached about 850 μA cm^{-2}, which is nearly four times of the Fe_2O_3 without FeOOH loading (Figure 4b). Conclusively, the existences of FeOOH cocatalysts help lower the overpotential of Fe_2O_3 photoanode and increase the photocurrent density significantly. Besides, both the Fe_2O_3 photoanode and Fe_2O_3/FeOOH photoanode showed stable current density after illuminated for 150 min. This also confirmed that the contact between FeOOH and Fe_2O_3 was well qualified even an external bias is applied.

Water splitting experiments (Figure S9, Supporting Information) at 0.43 V versus NHE (1.23 V vs RHE) were monitored using 100 mW cm^{-2} AM 1.5 G illumination to certificate whether the anodic photocurrent generated by the Fe_2O_3/FeOOH photoanode is the exclusive result of O_2 evolution. The PEC water splitting experiments were carried out for more than 70 h to make sure its long-term stability. The rate for O_2 evolution at the surface of Fe_2O_3/FeOOH photoanode was 10.1 μmol h^{-1} cm^{-2} (**Figure 5**b), while there was no obvious decay in this performance even after 70 h. This performance is comparable with $Co_3O_4/La_2Ti_2O_7$ (≈3 μmol h^{-1}, 2.5 h)[25] and $BaWO_xN_y$-$BaTaO_2N$ (≈11 μmol h^{-1}, 10 h)[26] photocells. Moreover, the stability of the devices was much better compared with the above mentioned samples. The high durability can be easily observed from the *I–t* curve for water splitting as shown in Figure 5c. The current density going steadily with time increasing, and only 4.4% decay occurred even after 70 h reaction. This can be attributed to the high quality of Fe_2O_3 prepared by PLD and the good contact between the nanostructured FeOOH and Fe_2O_3. The gas generation rates of H_2 and O_2 for the Fe_2O_3/FeOOH-Pt PEC device was nearly 2:1, indicating the photocurrent density come from pure water splitting in this system. The dark current of this PEC device was quite low and no gases were detected without light turned on. Plus, the amount of O_2 generated was in good agreement with half amount of the holes passing through the outer circuit (e^-/4, indicated by the broken line), indicating that the obtained photocurrent was derived from water splitting. A 97.3% Faradaic efficiency was calculated based on the amount of generated O_2 and the holes. This means nearly all the holes in the circuit were used for water oxidation.

Finally, monochromatic incident photo-to-electron conversion efficiency (IPCE) analysis of Fe_2O_3/FeOOH photoanode was processed in 1 M NaOH at 0.43 V versus NHE (1.23 V vs RHE) and the curve was shown in **Figure 6**. The IPCE decreased gradually with the wavelength increases. Light with wavelength below 600 nm make contribution to the photocurrent density of Fe_2O_3/FeOOH photoanodes, and the IPCE reached a maximum of 20.2% at 400 nm. Since the nanostructured FeOOH cannot change the absorption performance of Fe_2O_3 in the visible light region as discussed above, the trend of IPCE for Fe_2O_3/FeOOH photoanode was in good accordance with the absorption spectrum for bare Fe_2O_3 (Figure S7, Supporting Information).

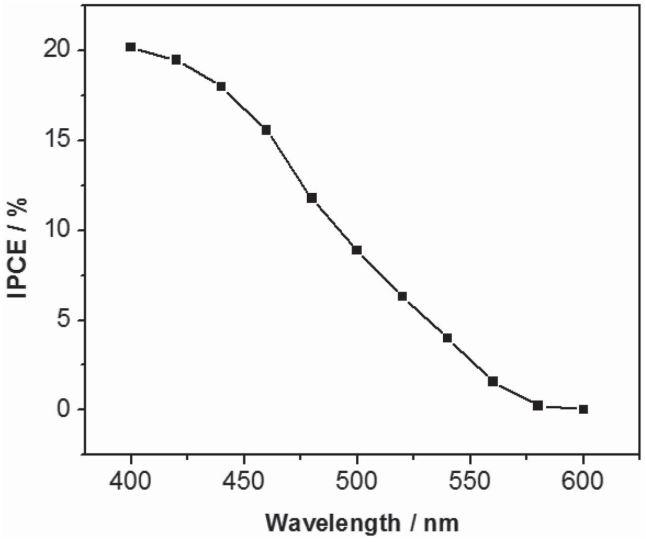

Figure 6. IPCE curve of Fe_2O_3/FeOOH photoelectrode at 0.43 V versus NHE.

3. Conclusion

The decorating of nanostructured FeOOH by photoelectrodeposition on the surface of hematite lead to an obvious decrease in the applied potential required to drive photoelectrochemical water oxidation as well as a great increase in the photocurrent density. The photocurrent onset potential shifted cathodically by 140 mV, and the photocurrent density increased to nearly four times at 0.43 V versus NHE (1.23 V vs RHE) compared to bare hematite photoanodes. This can be ascribed to the high reaction area for the nanostructured morphology and high electrocatalytic activity of FeOOH, which increased the amount of photogenerated holes involved in the water oxidation reaction and accelerates the kinetics of water splitting. Moreover, the gas generation rate of H_2 and O_2 for the Fe_2O_3/FeOOH-Pt PEC device was nearly 2:1, and the oxygen evolution rate for such prepared Fe_2O_3/FeOOH photoanode was as high as 10.1 μmol h^{-1} cm^{-2}. Furthermore, the high rate for water oxidation lasted for as long as 70 h with no obvious sigh of decay in the performance. As a result, we demonstrated the nanostructured FeOOH has great potential for application in PEC water oxidation as cocatalysts.

4. Experimental Section

Fe_2O_3 thin films were prepared by PLD method using a Fe_2O_3 pellet as the target and ITO as a substrate according to previous article.[19] The temperature for film deposition was 550 °C and the target was irradiated by laser for 20 min. After the laser irradiation, the film was kept at the same temperature in pure oxygen for 20 min. Such prepared hematite film had a thickness about 70 nm. Then nanostructured FeOOH were deposit on the Fe_2O_3 by photoelectrodeposition at 0.2 V versus Ag/AgCl in 0.1 M $FeSO_4$ solution. The light source was AM 1.5 G which is about 100 mW cm^{-2}.

Raman scattering spectra were measured using the Raman spectroscope (NRS-1000; Jasco Corp. Japan) equipped with an neodymium-doped yttrium aluminium garnet (Nd:YAG) laser (532 nm). The laser power is 1 mW. Field-emission scanning electron microscope (JSM-6701 F, JEOL) were used to characterize the morphology of the samples. Energy dispersive spectroscopy (SU8000, Hitachi Co., Japan) were used for element characterization. XPS experiments were performed in a Theta probe (Thermo Fisher) using monochromated Al Kα x-rays at $h\nu = 1486.6$ eV. Optical absorption properties of the Fe_2O_3 and FeOOH were measured through an UV–vis spectrophotometer (UV-2500PC; Shimadzu Co., Japan).

PEC measurements were obtained with an electrochemical station (ALS/CH model 650A) in a three-electrode mode. Platinum and saturated calomel electrode (SCE) were used as the counter electrode and reference electrode, respectively. AM 1.5 G solar simulation (WXS-80C-3 AM 1.5 G) with a light intensity of 100 mW cm^{-2} was utilized as the light sources directly without adding any light filter.

The solution for PEC measurements was 1 M NaOH aqueous.

Hydrogen and oxygen generation of the prepared Fe_2O_3/FeOOH photoanodes were measured using a water splitting system. FeOOH/Fe_2O_3 film with an area of 1 cm^2 on ITO (2 × 1 cm^2) was used. A 180 mL quantity of 1 M NaOH solution was put in a quartz glass cell (≈1.0 L). Then this glass cell was fixed on the water splitting system which was connected with a closed gas circulation system. There are three parts in the water splitting system including a vacuum line, a reaction cell, and a gas sampling port which were shown in Figure S9, Supporting Information. The generated H_2 and O_2 were in situ analyzed with a thermal conductivity detector (TCD) gas chromatograph (Shimadzu GC-8AIT, argon carrier). Similarly, AM 1.5 G solar simulation (WXS-80C-3 AM 1.5 G) with a light intensity of 100 mW cm^{-2} was utilized as the light sources directly without adding any light filter.

Supporting Information

Supporting Information is available from the Wiley Online Library or from the author.

Acknowledgements

Q.Y. and X.M. contributed equally to this work. This work received financial support from the World Premier International Research Center Initiative on Materials Nanoarchitectonics (WPI MANA), Japanese Government (Monbukagakusho: MEXT) Scholarship, National Basic Research Program of China (973 Program, 2014CB239301), and Japan Society for the Promotion of Science KAKENHI (Grant No. 24-02812).

Received: January 29, 2015
Revised: February 23, 2015
Published online: March 25, 2015

[1] C. Mao, F. Zuo, Y. Hou, X. Bu, P. Feng, *Angew. Chem., Int. Ed.* **2014**, *53*, 10485.
[2] I. S. Cho, M. Logar, C. H. Lee, L. Cai, F. B. Prinz, X. Zheng, *Nano. Lett.* **2014**, *14*, 24.
[3] a) Y. Hou, F. Zuo, A. Dagg, P. Feng, *Angew. Chem., Int. Ed.* **2013**, *52*, 1248; b) S. C. Warren, K. Voïtchovsky, H. Dotan, C. M. Leroy, M. Cornuz, F. Stellacci, C. Hébert, A. Rothschild, M. Grätzel, *Nat. Mater.* **2013**, *12*, 842.
[4] T. W. Kim, K. Choi, *Science* **2014**, *343*, 990.
[5] K. Maeda, D. Lu, K. Domen, *Angew. Chem., Int. Ed.* **2013**, *52*, 6488.
[6] M. Grätzel, *Nature* **2001**, *414*, 338.
[7] a) Y. Lin, G. Yuan, S. Sheehan, S. Zhou, D. Wang, *Energy Environ. Sci.* **2011**, *4*, 4862; b)Q. Yu, X. Meng, T. Wang, P. Li, L. Liu, K. Chang, G. Liu, J. Ye, *Chem. Commun.* **2015**, *51*, 3630.
[8] L. A. Marusak, R. Messier, W. B. White, *J. Phys. Chem. Solids* **1980**, *41*, 981.

[9] Y. Lin, Y. Xu, M. T. Mayer, Z. I. Simpson, G. McMahon, S. Zhou, D. Wang, *J. Am. Chem. Soc.* **2012**, *134*, 5508.
[10] A. Kay, I. Cesar, M. Grätzel, *J. Am. Chem. Soc.* **2006**, *128*, 15714.
[11] M. G. Walter, E. L. Warren, J. R. McKone, S. W. Boettcher, Q. Mi, E. A. Santori, N. S. Levis, *Chem. Rev.* **2010**, *110*, 6446.
[12] Y. Hu, S. Kleriman, G. D. Stucky, E. W. McFarland, *Chem. Commun.* **2009**, *19*, 2652.
[13] C. C. L. McCrory, S. Jung, J. C. Peters , T. F. Jaramillo, *J. Am. Chem. Soc.* **2013**, *135*, 16977.
[14] S. Tilley, D. M. Cornuz, K. Sivula, M. Grätzel, *Angew. Chem.* **2010**, *122*, 6549.
[15] B. Klahr, S. Gimenez, F. Fabregat-Santiago, J. Bisquert, T. W. Hamann, *J. Am. Chem. Soc.* **2012**, *134*, 16693.
[16] K. M. H. Young, T. W. Hamann, *Chem. Commun.* **2014**, *50*, 8727.
[17] C. Du, X. Yang, M. T. Mayer, H. Hoyt, J. Xie, G. McMahon, G. Bischoping, D. Wang, *Angew. Chem. Int. Ed.* **2013**, *52*, 12692.
[18] a) W. D. Chemelewski, H. Lee, J. Lin, A. J. Bard, C. B. Mullins, *J. Am. Chem. Soc.* **2014**, *136*, 2843; b) R. Alben, D. Weaire, J. E. Smith, M. H. Brodsky, *Phys. Rev. B* **1975**, *11*, 2271; c) B. Ludovic, N. Delphine, R. Solenn, M. Judith, S. Mandana, *J. Nano Res.* **2009**, *8*, 147.
[19] J. Cao, T. Kako, N. Kikugawa, J. Ye, *J. Phys. D: Appl. Phys.* **2010**, *43*, 325101.
[20] F. L. Formal, M. Grätzel, K. Sivula, *Adv. Funct. Mater.* **2010**, *20*, 1099.
[21] a) J. F. Zang, S. J. Bao, C. M. Li, H. J. Bian, X. Q. Cui, Q. L. Bao, C. Q. Sun, J. Guo, K. R. Lian, *J. Phys. Chem. C* **2008**, *112*, 14843; b) A. D. Fabio, A. Giorgi, M. Mastragostino, F. Soavi, *J. Electrochem. Soc.* **2001**, *148*, A845.
[22] S. C. Riha, B. M. Klahr, E. C. Tyo, S. Seifert, S. Vajda, M. J. Pellin, T. W. Hamann, A. B. F. Martinson, *ACS Nano* **2013**, *7*, 2396.
[23] L. Steier, I. H. Cardona, S. Gimenez, F. F. Santiago, J. Bisquert, S. D. Tilley, M. Grätzel, *Adv. Funct. Mater.* **2014**, *24*, 7681.
[24] M. Shao, F. Ning, M. Wei, D. G. Evans, X. Duan, *Adv. Funct. Mater.* **2014**, *24*, 580.
[25] J. Feng, W. Luo, T. Fang, H. Lv, Z. Wang, J. Gao, W. Liu, T. Yu, Z. Li, Z. Zou, *Adv. Funct. Mater.* **2014**, *24*, 3535.
[26] K. Maeda, D. Lu, K. Domen, *Angew. Chem., Int. Ed.* **2013**, *52*, 6488.